Atomic-scale topographic and friction force imaging and cantilever dynamics in friction force microscopy

Yaxin Song and Bharat Bhushan*
Nanotribology Laboratory for Information Storage and MEMS/NEMS, The Ohio State University, 650 Ackerman Road, Columbus, Ohio 43202, USA

(Received 2 February 2006; revised manuscript received 5 June 2006; published 2 October 2006)

Friction force microscopy (FFM) is commonly used for micro-, nano-, and atomic-scale topographic and friction (lateral) force imaging of surfaces. The experimental-obtained topographic and friction force images are closely correlated to the cantilever dynamics since in FFM, the normal and lateral forces between the cantilever tip and sample surface are measured from the cantilever flexural and twist angles. To understand the cantilever dynamics under tip-surface interaction and its effects on the measured topographic and friction force maps, efficacious models that can accurately simulate the cantilever behavior in operating conditions of FFM are essential. In this paper, a three-dimensional (3D) finite element (FE) beam model is employed to simulate the atomic-scale topographic and friction force profiling process in FFM. The tip-sample interaction forces are modeled as the interatomic forces between the tip and sample surface. It is identified that the topographic and lateral force maps obtained in FFM experiments are the combined results of the real spatial distributions of 3D tip-sample interatomic forces and cantilever dynamics. The experimental-obtained hexagonal (full atomic structure) and trigonal (atomic resolution of every other atom) topographic images of graphite surfaces are reproduced in simulations with different combinations of cantilever geometries, applied normal loads, and scan directions. Based on the simulated results, the methods to realize the observation of the full atomic structure of graphite are discussed.

DOI: 10.1103/PhysRevB.74.165401 PACS number(s): 68.35.Ja, 07.79.Sp, 68.35.Af, 68.35.Bs

I. INTRODUCTION

Atomic force microscopy (AFM) is commonly used for micro-, nano-, and atomic-scale surface imaging. Atomic-scale topographic imaging has been carried out by researchers on highly oriented pyrolytic graphite (HOPG) and other samples. Binnig *et al.*[1] successfully observed the hexagonal structure of graphite surface [see Fig. 1(a)]. In their experiment, a cantilever without tip was scanned over the graphite surface with its corner touching the surface to obtain the topographic images. Marti *et al.*[2] also obtained the full hexagonal topographic image of graphite surface covered with paraffin oil using a diamond epoxied to one of the four cross points of four platinum wires. However, many others[3,4] could only show the trigonal lattice of three peaks with a distance of about 0.246 nm in their experimentally-obtained topographic images, i.e., so called "atomic resolution of every other atom" [refer to Fig. 1(b)].

The possible reasons for the "atomic resolution of every other atom" in topographic maps of graphite have been studied by researchers. Some believe that it is due to the asymmetric atomic structure of graphite lattices, i.e., the existence of two different types of atoms. Whereas the tip-surface forces calculated using interatomic potential have showed that the force difference for the two types of atoms is very small and both of them should be visible.[5,6] It is generally recognized that stick-slip will occur if a soft AFM cantilever is scanned over a surface with large lateral forces, or equivalently, under large applied normal loads.[7–10] The occurrence of stick-slip tip motion has been considered to be the reason for the measurement of topography images of every other atom.[11] With different combinations of cantilever lateral stiffnesses and normal loads, simulations on AFM cantilever behavior in measurements should be able to obtain the hexagonal (full atomic structure) or trigonal (resolution of every other atom) topography maps as obtained in the experiments. However, this has not yet been demonstrated in the previous numerical simulations considering cantilever deflection.

Atomic-scale stick-slip was observed by Mate *et al.*[7] in their measurement of atomic-scale friction between a tungsten wire and graphite surface using a friction force microscopy (FFM). With an optical beam-deflection FFM, Ruan and Bhushan[4] simultaneously measured the topography and friction force maps of graphite surfaces and the stick-slip tip motion during measurement was also observed, as shown in Fig. 1(c). This stick-slip tip motion, as well as the scan direction in FFM have significant effects on the measured topographic and lateral force maps.[8–10] In FFM, the normal and lateral forces between the cantilever tip and surface are measured from the cantilever flexural and twist angles. Therefore, topographic and lateral force images obtained using FFM are closely correlated to the cantilever response. Efficacious models that can accurately simulate the cantilever behavior in operating conditions of FFM are essential for the understanding of cantilever dynamics and the effects of cantilever geometry, applied normal load, and scan direction on the measured topographic and lateral force maps.

AFM cantilevers can be modeled as a three-dimensional (3D) beam with the clamped-free boundary conditions, which has four deformation shapes: vertical bending (bending about the y axis), lateral bending (bending about the z axis), torsion (about the x axis), and extension (along the x axis), as shown in Fig. 2. Point-mass models[12] and one-dimensional (1D) beam models[13–15] have been employed to model cantilever vertical bending behavior. The cantilever torsion is usually modeled by torsional shaft models.[16–20]

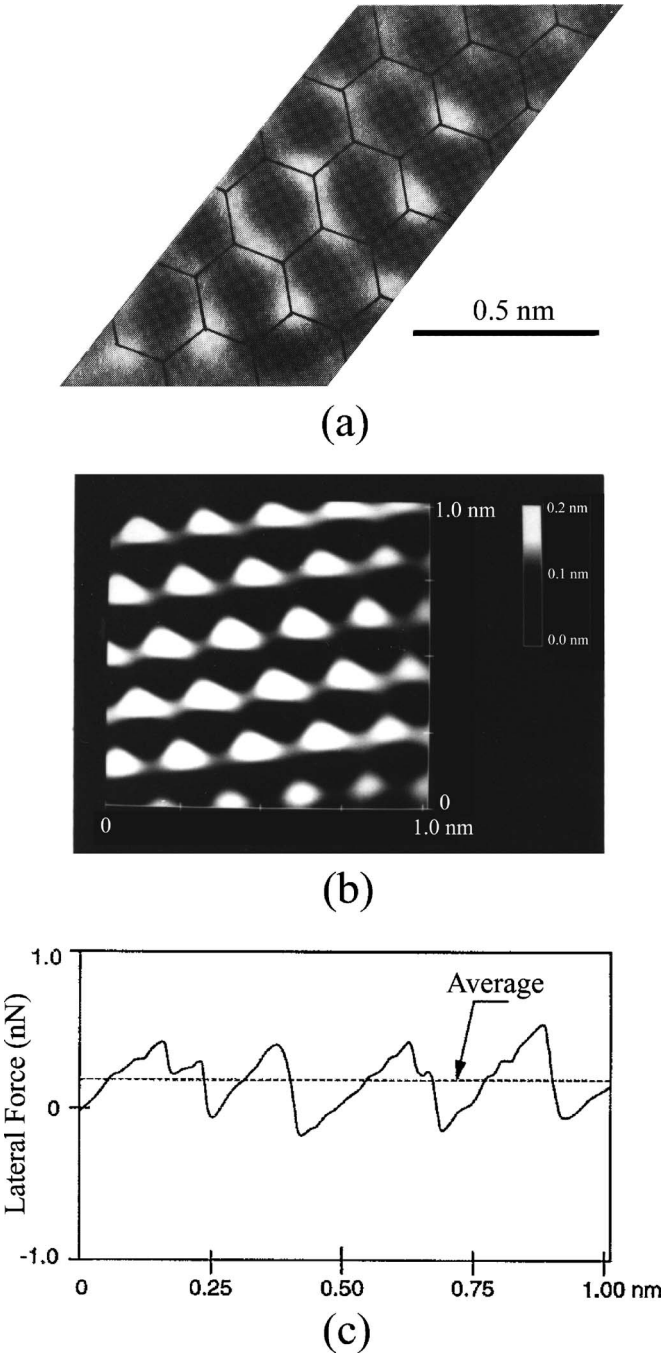

FIG. 1. AFM Topography images of graphite surface and typical line plot of friction profile. (a) Topography image of graphite obtained with a cantilever with tip (Ref. 1). Hexagonal structure of graphite surface is shown. (b). Topography map of HOPG shown atomic resolution of every other atoms (Ref. 4). (3) Stick-slip tip motion in friction measurements (Ref. 4).

The coupled torsional-bending model, which considers the coupling between torsion and lateral bending of the cantilever, was developed by Song and Bhushan.[21] The cantilever in FFM undergoes vertical bending, torsion, and lateral bending. For the simulation of friction profiling process, two models exist to date with cantilever deflections taken into consideration. Sasaki *et al.*[8] constructed a total potential energy consisting of the elastic energy of cantilever and sample

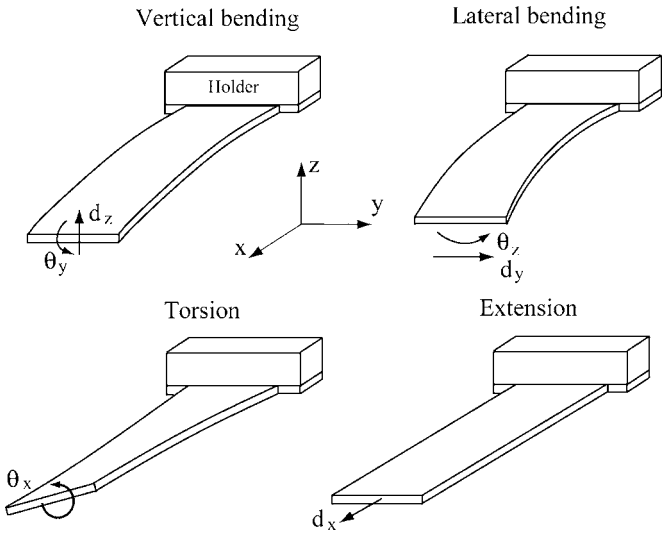

FIG. 2. Four deformation shapes of a rectangular cantilever in FFM.

surface and potential of tip-sample interaction. Polak-Ribiere-type conjugate gradient method was then employed to minimize the total potential to obtain the tip position with a fixed tip-surface distance. This model is a static model which does not consider the dynamic effects of the cantilever response in friction profiling process. Hölscher *et al.*[9,11,22] simulated the tip motion during the profiling process using a 3D point-mass model. They showed that the friction force maps of graphite surface represent a "hollow-site resolution" instead of "atomic resolution" because of the two-dimensional (2D) stick-slip movement of the tip.[11] Using the same point-mass model, Wang *et al.*[23] studied the profiling process in FFM and believed that the topographic maps obtained in FFM measurements were, instead of the constant normal load profiles, the maps of the maxima of the longitudinal direction lateral force. In the 3D point-mass model, the tip-cantilever system is represented by three masses connected by elastic springs to its holder. The point-mass model has three uncoupled translational degrees of freedom (DOFs). In each translational direction, the motion of the point-mass is described as a single DOF oscillator. The friction force in that direction is obtained as the product of the translational displacement (relative to the holder) of the mass and the spring stiffness. As a mathematical approximation of the real tip-cantilever system, this model's parameters (effective masses and spring stiffnesses) can only be obtained by estimation and the simulated responses are translational displacements instead of the rotation angles detected in FFM. Furthermore, the 3D point-mass model neglects the coupling between the lateral bending and torsion of the FFM cantilever, which could have significant effects on cantilever response.[21]

Recently, Song and Bhushan[24] developed a 3D finite element (FE) beam model for numerical simulation of free and surface-coupled dynamics of tip-cantilever system in various dynamic AFM modes. Representing the cantilever by 3D beam elements, this versatile model can address the exact excitation mechanisms, tip geometry/location, tilting of the

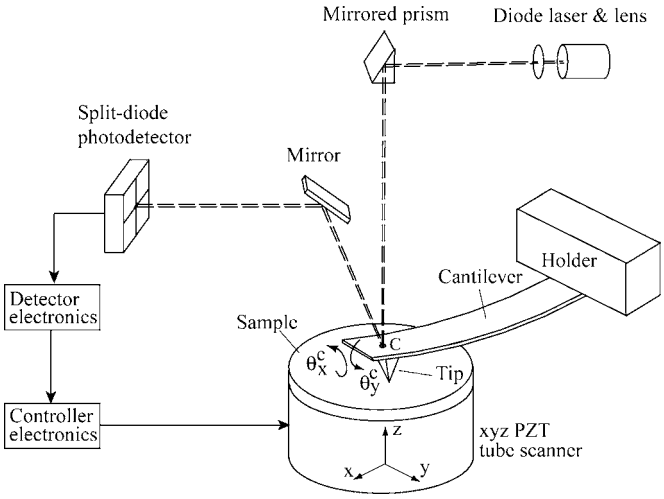

FIG. 3. Schematic diagram of a FFM. The four-segment photodiode can measure the flexural angle θ_y^C and twist angle θ_x^C of the cantilever at the location close to the tip (point C). θ_y^C is related to the vertical bending caused by normal load. θ_x^C is the twist angle due to lateral force along the fast scan direction. By maintaining a constant θ_y^C with a feedback loop, topography of the sample surface can be measured.

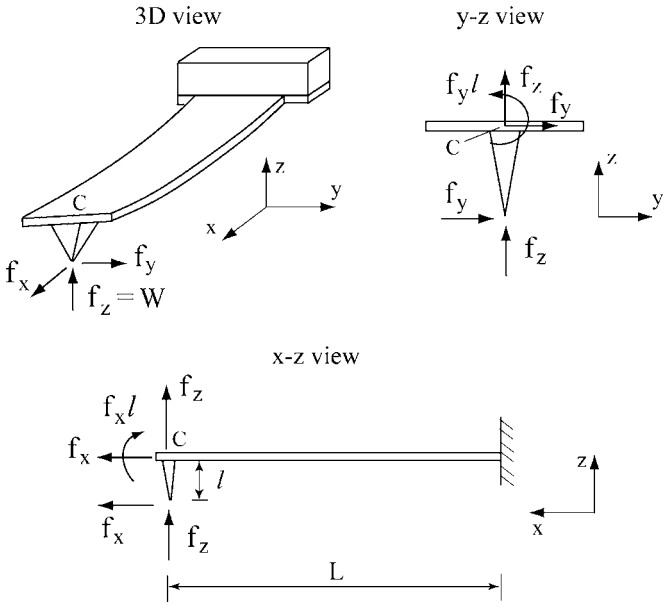

FIG. 4. 3D tip-surface interaction forces on cantilever tip and the resulting forces and moments on cantilever. Normal force f_z and the moment $M_y^C = -f_x l$ due to the lateral force f_x is responsible for the vertical bending of the cantilever. Extension is caused by the lateral force f_x. Lateral force f_y cause the lateral bending, and the resulting torque $f_y l$ twists the cantilever.

cantilever to the sample surface, and all the possible couplings among the different deflections of the AFM cantilever. Compared with the point-mass model, this FE model represents a more realistic tip-cantilever model: the model's parameters can be determined from the cantilever geometry and material properties; translational displacements, as well as flexural and twist angles are the simulated cantilever responses.

In this paper, we use the 3D FE beam model to simulate the atomic-scale topographic and lateral force profiling process in FFM. First, the working mechanism of a FFM and the cantilever deflections during profiling process are described. Then, we illustrate how to simulate the FFM cantilever response to the interatomic forces between tip and graphite surface. Atomic-scale topographic and friction force maps on graphite surface are obtained for different combinations of cantilever geometries, applied normal loads, and scan directions. The simulated results are compared with the experimental results and the reasons that the full atomic structure of surfaces is detected or not are discussed.

II. CANTILEVER DEFLECTIONS IN FFM

Figure 3 shows a schematic diagram of the optical beam-deflection FFM.[25,26] The optical beam-deflection FFM allows the simultaneous measurements of surface topography, normal and lateral forces. A laser beam is projected on the upper surface of the cantilever at a point close to the tip (point *C*). The beam is reflected and led by a mirror into a four-segment photodiode. By calibrating the vertical and lateral voltage output of the photodiode, the cantilever flexural angle θ_y^C and twist angle θ_x^C are measured, respectively. θ_y^C and θ_x^C are the only deflection information we can obtain from the FFM measuring system. Figure 4 shows the 3D tip-surface interaction forces exerted on the cantilever. With the tilting of the cantilever to the sample surface being neglected, the vertical bending is solely caused by the normal force f_z and the moment $M_y^C = -f_x l$ resulting from the lateral force f_x, where x is the longitudinal axis of the cantilever, l is the length of the tip. The lateral force f_y causes the lateral bending, and its resulting torque $f_y l$ twists the cantilever. Extension occurs due to the lateral force f_x but usually it is very small and thus can be neglected. For a typical cantilever, the extension stiffness is 4-5 orders of magnitude higher than that of vertical bending.

Refer to Figs. 2 and 4, θ_y^C is the flexural angle of the cantilever due to vertical bending. It is related to the normal load f_z and lateral force f_x. We will demonstrate below that the contribution from f_x to θ_y^C is much smaller than that from f_z (less than 5%). Approximately, the normal load f_z can be viewed as the sole cause of θ_y^C. Therefore, normal force f_z can be obtained by measuring θ_y^C. With the help of a feedback loop in FFM, surface topography (or constant normal force profile) can be obtained by keeping a constant θ_y^C through the z-direction motion of the piezotube when the cantilever tip is scanned over the sample surface. Since the lateral force f_y is the only interaction force that is responsible for the cantilever torsion, the twist angle θ_x^C is a good measurement for f_y.

In constant-force mode of FFM, a constant normal load (or, equivalently, a constant θ_y^C) is maintained to make the measured results meaningful. During the measurement, the (fast) scan direction is perpendicular to the longitudinal direction of the cantilever (along the y axis) and the lateral force f_y is obtained by measuring the twist angle θ_x^C. During measurement, the tip is always in a stable equilibrium state

in the vertical direction if the holder is moving with a moderate scan speed. In that case, the vertical displacement and flexural angle can be obtained by

$$d_z^C = \text{constant} = \frac{L^3}{3EI_y} f_z + \frac{L^2 l}{2EI_y} f_x, \tag{1a}$$

$$\theta_y^C = \text{constant} = -\frac{L^2}{2EI_y} f_z - \frac{Ll}{EI_y} f_x, \tag{1b}$$

where E is Young's modulus, L is cantilever length, I_y is moments of inertia about the y axis, respectively. For a rectangular cantilever, $I_y = bh^3/12$, where b is width, h is thickness of the cantilever cross section. For a typical cantilever, the tip length l is about 1/10–1/30 of the cantilever length L. The lateral force f_x could be one order of amplitude smaller than the normal force f_z. Refer to Eq. (1), the contribution of f_x to d_z^C and θ_y^C is much smaller than that from f_z. With the contribution of f_x being neglected, we have $d_z^C \approx \frac{L^3}{3EI_y} f_z$ and $\theta_y^C \approx -\frac{L^2}{2EI_y} f_z$. Therefore, the topography map obtained in FFM $z_t(x_t, y_t)$ can be obtained by solving the nonlinear equation

$$f_z(x_t, y_t, z_t) = W, \tag{2}$$

where (x_t, y_t, z_t) are coordinates of cantilever tip, W is applied normal load.

Based on the above discussion, we note that the contribution of f_x to cantilever vertical bending is much smaller than that from f_z. Thus, the topography should reflect more about the variation of f_z than that of f_x. In addition, since θ_y^C is the only deflection information that the FFM feedback system can use to keep a constant normal load, the scan direction in constant-force mode of FFM could only be in the y axis of the cantilever. During scanning, only the lateral force f_y can be measured through the twist angle θ_x^C.

III. TOPOGRAPHIC AND FRICTION FORCE MAPS OF GRAPHITE WITHOUT CONSIDERING CANTILEVER DYNAMICS

The simulation of FFM topography and friction force maps involves the calculation of the forces exerted on the tip, which are functions of tip position with respect to the sample surface, and the cantilever deflections due to those forces. The interaction forces can be calculated from the spatial derivatives of an interaction potential. The forms of the interaction potential depend on the adopted atomistic model for tip and sample surface. In this paper, a simplified model is adopted to calculate the interatomic forces between cantilever tip and graphite surface. The tip is represented by a one-atom model and the relaxation of the tip and sample surface is neglected. It is assumed that the interaction system is always in an equilibrium state since the scan speed of the cantilever tip in FFM is much lower than the characteristic velocity of the lattice vibration.

There are complex tip-surface models in which multi-atom tip models are employed and the relaxation of tip and surface is considered.[27] The tip-surface forces in these models are calculated using the molecular dynamics, or static atomistic simulation and quantum mechanical techniques. These models, which describe the motion of single atoms, can address the tip and surface deformations and even the contamination of the tip by a cluster of surface material. However, molecular dynamics techniques and quantum mechanical methods are still too expensive for routine image modeling. The practical time length of simulation is several orders of magnitude smaller than the time length in a typical scanning process. Static methods based on total energy minimization are only suited for modeling very slow adiabatic processes at low temperature. In our simulations, the simplified model is employed so that we can put our emphasis on the effects of cantilever dynamics on FFM images.

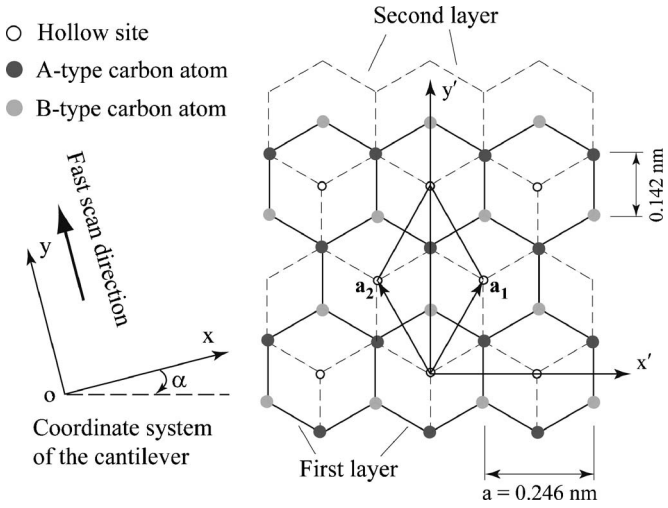

FIG. 5. 2D schematic view of the periodic hexagonal lattice structure of (0001) graphite surface. Two layers of honeycomb structures are shown. Two types of carbon atoms, *A*-type and *B*-type, exist due to the way the layers staggered. *A*-type atoms have a direct neighbor in the adjacent layers while *B*-type atoms do not. Hollow sites are the centers of each hexagon. In the coordinate system for the cantilever, the x axis is along the cantilever longitudinal direction. The cantilever is always scanned along the y axis (perpendicular to the longitudinal direction of the cantilever) in constant-force mode of FFM. Another coordinate system (x', y') is introduced for convenient determination of atom locations on the graphite surface. The shown parallelogram is a primitive unit cell which includes two carbon atoms. Vectors $\mathbf{a}_1$ and $\mathbf{a}_2$ are the unit lattice vectors for the primitive unit cell. The angle α is defined to represent the relation between the coordinate systems for the cantilever and graphite lattice structure.

Figure 5 shows the hexagonal structure of (0001) graphite surface. Layers of the hexagonal structures are staggered with a distance of 0.335 nm. The periodic structure of the graphite surface induces a periodic interaction potential,[4] which can be approximated by the Lennard-Jones potential in the form of $V_{ts}(\mathbf{r}_t) = \Sigma_k \Sigma_i 4\varepsilon_{ts}[(\sigma/r_{ki})^{12} - (\sigma/r_{ki})^6]$. Here, the parameters are chosen as $\varepsilon_{ts} = 0.87 \times 10^{-2}$ eV and $\sigma = 0.249$ nm (see Ref. 8), r_{ki} is the distance from the kth atom on the tip to the ith atom on the surface ($k=1$ in our one-atom tip model). In the (x, y, z) coordinate system of the cantilever, the tip position vector is denoted as $\mathbf{r}_t = (x_t, y_t, z_t)$.

We define α as the angle from the x axis of the cantilever to the x' axis of the graphite surface. Using a one atom tip

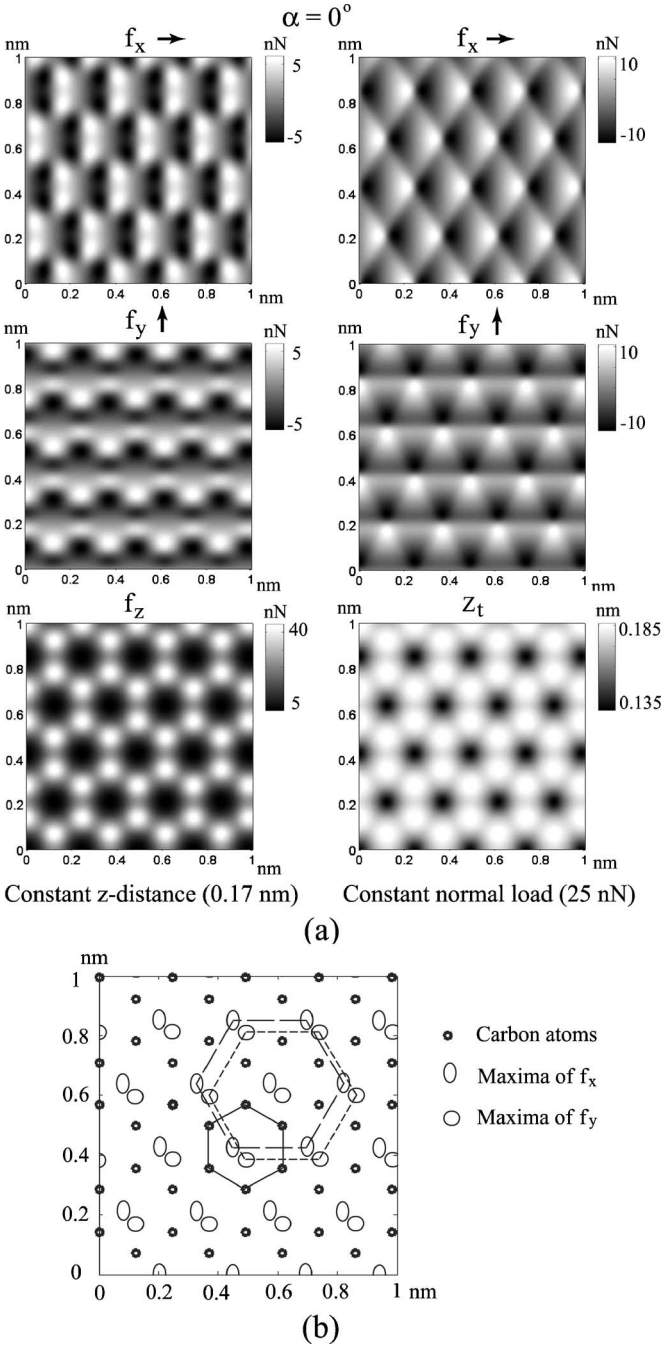

FIG. 6. (a) 3D interatomic force maps with a constant tip-surface distance z_t=0.17 nm (left-hand column) and lateral interatomic force and tip-surface distance maps with a constant normal load f_z=25 nN (right-hand column). (b) The relative positions of the carbon atoms and the maxima of lateral forces under the constant normal load f_z=25 nN.

model, interaction force maps are calculated for a constant tip-surface distance z_t=0.17 nm when α=0°, as shown in the left-hand column of Fig. 6(a). If the normal force keeps constant, z_t has to change at different locations on the graphite surface. For a constant normal load W=25 nN, nonlinear equation in (2) is solved to get the proper z_t map and the corresponding lateral force maps are then calculated. The maps in the right-hand column of Fig. 6(a) give the tip-surface distance and lateral forces exerted on the cantilever tip when the tip is at different locations of the graphite surface. The topography of the graphite surface can be obtained from z_t map by subtracting the min(z_t) from z_t. The results in the right column of Fig. 6(a) can be viewed as the FFM topography and friction force maps of graphite surface with cantilever dynamics being neglected.

Figure 6(b) show the relative locations of the carbon atoms of graphite surface and the maxima of the lateral forces under the constant normal load W=25 nN. It is clear that without considering cantilever dynamics, the topographic map or constant normal force profile does reflect the surface atomic structure. The locations of the maxima of the normal force coincide to the atom locations. Whereas the lateral force maps are not straightforward tools for observation of atomic structures since the maxima of the lateral forces are not located at the atom locations.

We note that the horizontal and vertical axes of the maps in Fig. 6(a) are the x and y coordinates of the cantilever tip at time t, i.e., $(x_t(t), y_t(t))$. In the topographic and friction maps measured by FFM, the horizontal and vertical axes represent actually the "nominal" coordinates of the tip position, i.e., the tip position at time t if the cantilever is rigid (no deflection). The nominal tip coordinates are determined from the coordinate of the cantilever holder. Here we represent them as $(x_h(t)+L_h, y_h(t))$, where $(x_h(t), y_h(t))$ are coordinates of the holder and L_h is a constant in each experiment. Due to the cantilever deflection during measurement, usually one will find $(x_t(t), y_t(t)) \neq (x_h(t)+L_h, y_h(t))$.

In addition, in the simulation for the topography map shown in Fig. 6(a), with or without considering the contribution from f_x, the resulting topography is almost the same. This proves again that the contribution of f_x to cantilever vertical bending is very small compared to that from f_z and can be neglected.

IV. CANTILEVER RESPONSE SIMULATION

We use the 3D finite element beam model developed earlier[24] to describe the cantilever motion in a FFM. In this model, the cantilever is discretized by 3D beam elements. At the nodes of each beam element, there are six degrees of freedom (DOFs): three translational and three rotation angles. In the (x, y, z) coordinate system shown in Figs. 2–4, the motion equation governing the cantilever response is expressed as

$$\mathbf{M}\ddot{\mathbf{u}}_{\text{tol}} + \mathbf{C}\dot{\mathbf{u}} + \mathbf{K}\mathbf{u} = \mathbf{F}_{\text{ts}}. \tag{3}$$

Here, $\mathbf{M}$ and $\mathbf{K}$ are mass and stiffness matrices, $\ddot{\mathbf{u}}_{\text{tol}}$ ($\mathbf{u}_{\text{tol}}$) is the acceleration (displacement) vector of the cantilever, $\mathbf{u}$ and $\dot{\mathbf{u}}$ are, respectively, the displacement and velocity vectors of the cantilever relative to its holder, $\mathbf{F}_{\text{ts}}$ is tip-sample interaction force vector. The displacement vector of the cantilever holder is expressed as $\mathbf{g}_{\text{h}}=\{x_h, y_h, z_h\}^{\text{T}}$. The displacement vector $\mathbf{u}_{\text{tol}}$ is related to the relative displacement vector $\mathbf{u}$ by

$$\mathbf{u}_{\text{tol}} = \mathbf{u} + \mathbf{\Gamma}\mathbf{g}_{\text{h}}, \tag{4}$$

where $\mathbf{\Gamma}$ is the position matrix to describe the relation between the displacement vectors $\mathbf{u}_{\text{tol}}$ and $\mathbf{u}$. Rewriting the mo-

tion equation in (3) in the reference frame attached to the cantilever holder, we have

$$\mathbf{M}\ddot{\mathbf{u}} + \mathbf{C}\dot{\mathbf{u}} + \mathbf{K}\mathbf{u} = \mathbf{F}_{\text{ts}} - \mathbf{M}\boldsymbol{\Gamma}\ddot{\mathbf{g}}_{\text{h}}. \tag{5}$$

In our simulation, it is assumed that the cantilever tip is located at the end of the cantilever. For easy illustration and to save computational time, in the following of this paper, the cantilever is represented by only one 3D beam element. With a moderate scan speed, the cantilever deflections in FFM profiling process are dominated by its first-order vibrational modes corresponding to vertical bending, torsion, and lateral bending. The fact that the cantilever is discretized by only one beam element will not compromise the simulation accuracy significantly, which has been confirmed in our trial simulations where the cantilever is discretized with ten 3D beam elements. In the reference frame attached to the cantilever holder, there are six DOFs at the end of the cantilever, i.e., $\mathbf{u}=\{d_x^C, d_y^C, d_y^C, \theta_x^C, \theta_y^C, \theta_z^C\}$. The position vector is

$$\boldsymbol{\Gamma} = \begin{bmatrix} 1 & 0 & 0 & 0 & 0 & 0 \\ 0 & 1 & 0 & 0 & 0 & 0 \\ 0 & 0 & 1 & 0 & 0 & 0 \end{bmatrix}^{\text{T}}. \tag{6}$$

The extension of the cantilever can be neglected, i.e., $d_x^C=0$. In constant-force mode of FFM, vertical bending-related DOFs d_y^C and θ_y^C are determined by Eq. (1). The cantilever deflections corresponding to lateral bending (d_y^C and θ_z^C) and torsion (θ_x^C) are governed by Eq. (5). We consider the cantilever is scanned with a constant velocity, i.e., $\ddot{\mathbf{g}}_{\text{h}}=\{0,0,0\}^{\text{T}}$. Equation (5) is then expressed as

$$\begin{aligned} &\rho AL \begin{bmatrix} 39/105 & 0 & -11L/210 \\ 0 & I_p/3A & 0 \\ -11L/210 & 0 & L^2/105 \end{bmatrix} \begin{Bmatrix} \ddot{d}_y^C \\ \ddot{\theta}_x^C \\ \ddot{\theta}_z^C \end{Bmatrix} \\ &+ \begin{bmatrix} c_{11} & c_{12} & c_{13} \\ c_{21} & c_{22} & c_{23} \\ c_{31} & c_{32} & c_{33} \end{bmatrix} \begin{Bmatrix} \dot{d}_y^C \\ \dot{\theta}_x^C \\ \dot{\theta}_z^C \end{Bmatrix} \\ &+ \begin{bmatrix} 12EI_z/L^3 & 0 & -6EI_z/L^2 \\ 0 & GJ/L & 0 \\ -6EI_z/L^2 & 0 & 4EI_z/L \end{bmatrix} \begin{Bmatrix} d_y^C \\ \theta_x^C \\ \theta_z^C \end{Bmatrix} = \begin{Bmatrix} f_y^C \\ M_x^C \\ M_z^C \end{Bmatrix}, \end{aligned} \tag{7}$$

where G is shear modulus, ρ is mass density, A is area of cross section, J is torsion constant. For a cantilever with a rectangular cross section, $J \approx \frac{1}{3}bh^3\left[1.0-0.630\frac{h}{b}+0.052\left(\frac{h}{b}\right)^5\right]$. The force and moments at point C are related with f_y as

$$\begin{Bmatrix} f_y^C \\ M_x^C \\ M_z^C \end{Bmatrix} = \begin{Bmatrix} 1 \\ l \\ 0 \end{Bmatrix} f_y(x_t, y_t, z_t). \tag{8}$$

The lateral force f_y is a function of the tip location. Tip location can be determined from Eq. (2) and the following equations

$$x_t = x_h + L - l\theta_y^C, \tag{9a}$$

$$y_t = y_h + d_y^C + l\theta_x^C. \tag{9b}$$

In Eq. (9a), we note that $-l\theta_y^C \approx \frac{L^2 l}{2EI_y} f_z$=constant, i.e., along each scan line, x_t=constant. Observing Eqs. (7)–(9), it is clear that the lateral bending and torsion of the cantilever are coupled together since y_t is dependent on both d_y^C and θ_x^C. Equation (7) is nonlinear and needs to be solved numerically with Eq. (2) to simulate the cantilever response in FFM. The resulting maps of z_t and θ_x^C are the FFM imaging results of topography and friction force, respectively.

The damping matrix in Eq. (7) addresses the energy dissipation mechanism in the tip-cantilever-surface system. It consists of two parts. One is the damping that the cantilever encounters when it is far away from the sample surface, including the material damping inside the cantilever and that from the air if it is not operated in vacuum. The other part is induced from the tip-sample interaction, such as phonon generation. Song and Bhushan[24] has demonstrated that the damping effects due to the tip-sample interaction can be equivalently addressed as an additional damping term to the material damping matrix of the cantilever. Here, the damping matrix is calculated as[24]

$$\mathbf{C} = [\boldsymbol{\phi}_1, \boldsymbol{\phi}_2, \boldsymbol{\phi}_3]^{-\text{T}} \,\text{diag}(2\varsigma_1\omega_1, 2\varsigma_2\omega_2, 2\varsigma_3\omega_3)[\boldsymbol{\phi}_1, \boldsymbol{\phi}_2, \boldsymbol{\phi}_3]^{-1}, \tag{10}$$

where ω_i, $\boldsymbol{\phi}_i$ and ς_i ($i=1,2,3$) are the ith natural circular frequency, normalized eigenmode vector and damping ratio of the system. Usually, large damping ratios (close to 1.0) are adopted to simulate the damping effects in the profiling process of FFM.

V. RESULTS AND DISCUSSION

We simulated the profiling processes to obtain the topographic and lateral force maps of graphite surface for different combinations of normal loads, tip lengths, and scan directions. The rectangular silicon cantilever considered here has the following dimensional and material parameters: $L=252$ μm, $b=35$ μm, $h=2.3$ μm, $\rho=2330$ kg/m^3, $E=1.3\times10^{11}$ Pa, $\upsilon=0.28$. Two scan directions are considered. In one case, $\alpha=0°$, i.e., the scan is carried out along the y' axis, and in the other case $\alpha=30°$, which is equivalent to $\alpha=90°$ due to the hexagonal structure of graphite, i.e., the scan direction is along the x' direction. The scan size is 1 nm $\times$1 nm. The scan velocity in the fast scan direction is 200 nm/s. Figure 7 shows the simulated maps of the cantilever twist angle $-\theta_x^C$, the tip-distance map z_t, and the paths of cantilever tip. The maps of $-\theta_x^C$ can be viewed as a measurement of the lateral force that resists the movement of the cantilever, i.e., the lateral force whose direction is opposite to the scan direction. The effects of cantilever dynamics in FFM topography and friction images can be clearly demonstrated by comparison of the maps shown in Figs. 6 and 7.

A. Slow-fast motion pattern

In Fig. 7(a), the results are for the normal load $W=10$ nN, tip length $l=12.5$ μm, and $\alpha=0°$. The full hexago-

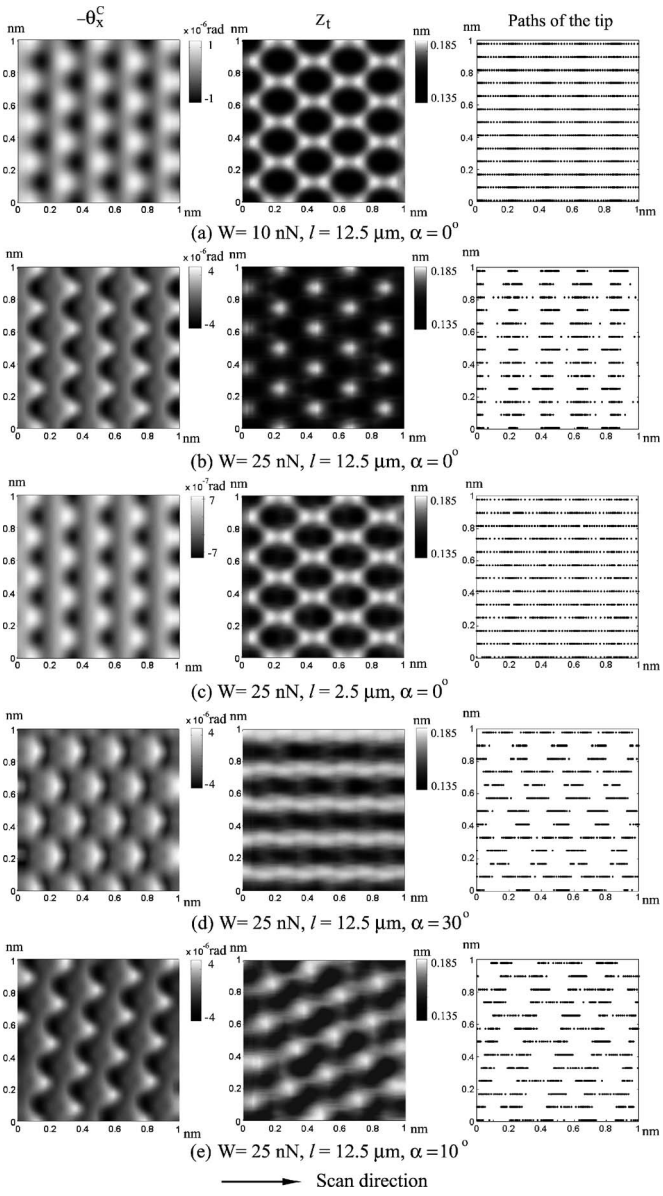

FIG. 7. The simulated maps of cantilever twist angle $-\theta_x^C$ (left-hand column) and tip-surface distance (middle column) z_t and 13 paths of the cantilever tip (right-hand column) for different combinations of the normal loads, tip lengths, and scan directions. The maps of cantilever twist angle are equivalent to the lateral force maps. The tip-surface distance maps are equivalent to the topographic maps. The data on the maps are unit-cell averaged. The paths of the tip is "time resolved," i.e., the paths are plotted by dots separated by equal time interval Δt=0.05 ms. The height variation in all topographic maps is about 0.03 nm, which agrees well with the experiment and theoretical calculation (Refs 29 and 30.)

nal structure of graphite surface can be seen in the topographic map. The paths of the cantilever tip are plotted by dots separated by equal time interval. Although the cantilever holder moves in a constant velocity, the cantilever tip does not slide over the surface smoothly. The dense part on the tip paths indicates that the tip is moving slowly over the surface while the sparse part represents a faster motion. As the "slow-fast" motion of the cantilever tip becomes remarkable,

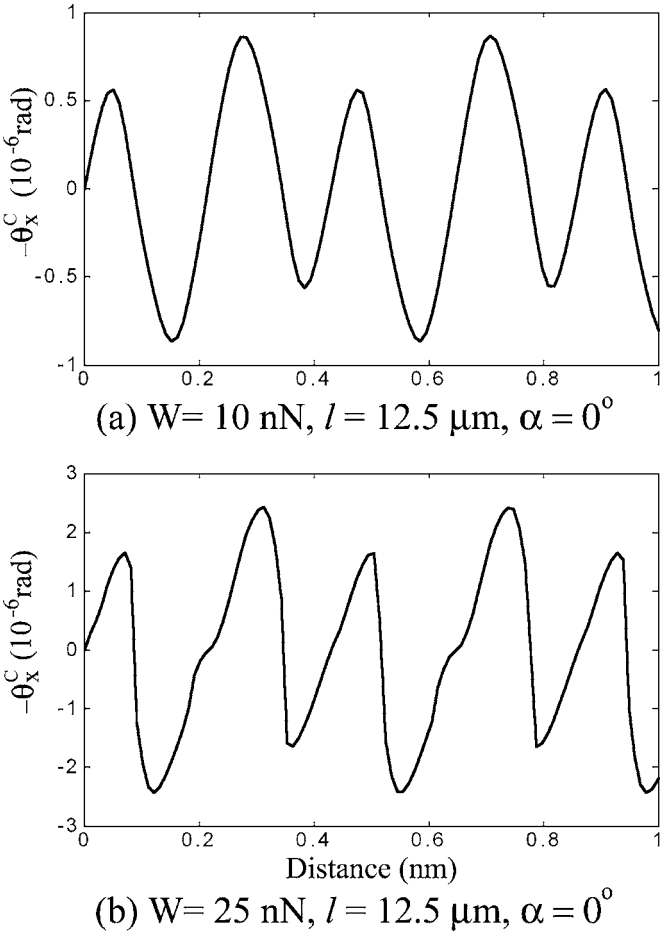

FIG. 8. Plots of cantilever twist angles for the scan lines of x_t =0.172 nm under two different normal loads, i.e., the third paths in Figs. 7(a) and 7(b).

many researchers refer it as "stick-slip" motion. Figure 7(b) gives the results under the same conditions as those in Fig. 7(a), except that the normal load is increased from 10 nN to 25 nN. The slow-fast tip motion in Fig. 7(b) is more remarkable than that in Fig. 7(a) due to the increased normal load, as shown clearly in the tip paths in Figs. 7(a), 7(b), and 8. Consequently, the hexagonal structure in topography cannot be observed in Fig. 7(b) and only the "resolution of every other atom" is shown. Also, dramatic difference can be seen in the lateral force maps in Figs. 7(a) and 7(b).

The topographic and lateral force maps obtained in FFM measurements are the combined results of the real spatial distributions of 3D tip-sample interaction forces and cantilever dynamics. In the measured maps of FFM, the topography and lateral forces at the locations of the tip $(x_t(t), y_t(t))$ are plotted against the "nominal" coordinates of the tip $(x_h(t) + L_h, y_h(t))$. The discrepancy between the measured results and the realities depends on how close it is between $(x_t(t), y_t(t))$ and $(x_h(t) + L_h, y_h(t))$. The tip paths shown in Fig. 7 are different from the simulated results reported by Sasaki *et al.*[8] and Hölscher *et al.*[11] In their analyses, the cantilever tip follows a zigzag stick-slip motion, moving from one hollow site to another and staying most of the time there. In our simulations, the tip move straight along the scan lines due to

the constant normal load condition. Refer to Eq. (9a), we have $x_t = x_h + L - l\theta_y^C = \text{constant}$. Therefore, in each scan line, it is the difference between $y_t(t)$ and $y_h(t)$ that determines the discrepancy between the measured results and the realities. The observation of surface atomic structure from the topographic maps is possible if the cantilever tip moves smoothly enough over the sample surface. Furthermore, from the tip paths shown in Fig. 7, the slowly-moving part of the tip paths could happen at the hollow sites or somewhere near the atom locations. It is not necessary true that the cantilever tip always stays more time at the hollow sites than other locations.

We note that in our simulation, the feedback system works instantaneously to keep the constant normal load condition. In reality this could not be possible. In experiment, the scan velocity should be small enough in order that the feedback system has enough time to react effectively to adjust the tip-sample distance even at the fast motion part of the tip paths.

B. Conditions of occurrence of remarkable slow-fast tip motion

One would ask under what circumstances remarkable slow-fast tip motion (or stick-slip) will not occur so that the detection of the full atomic structure becomes possible. It is generally recognized that stick-slip will occur if a soft cantilever is scanned over a surface with large lateral forces.[7–9] Fujisawa *et al.*[10] experimentally found that the sticking domain decreased with the increased normal load, and under lower normal load the tip shows smoother motion. Their observation are consistent to the conclusion that stick-slip occurs for soft cantilevers under large lateral forces since a high normal load means a smaller tip-sample distance and therefore larger lateral forces. Johnson and Woodhouse[28] assumed a sinusoidal lateral force and gave the analytical condition under which the tip motion is steady and no stick-slip occurs

$$T^* < T_c^* = \lambda k_e / 2\pi, \tag{11}$$

where T^* is the magnitude of the sinusoidal lateral force, T_c^* is the critical lateral force magnitude at which stick-slip will occur, λ is the periodic lattice spacing of the sample surface, k_e is the effective lateral stiffness. The effective lateral stiffness can be calculated from the expression $1/k_e = 1/k_{lat} + 1/k_{surf}$, where k_{lat} is the lateral cantilever stiffness considering both cantilever lateral bending and torsion, k_{surf} is the tip-surface contact stiffness. Here, since we always assume that the cantilever tip itself is rigid, k_{surf} is a description of atomic relaxation (or surface flexibility). Although Eq. (11) is obtained under the assumption of a sinusoidal lateral force, it may be used for a rough estimation of the occurrence of stick-slip in our simulations. For a rigid surface, k_e equals the lateral stiffness of the cantilever, i.e.

$$k_e = k_{lat} = \left(\frac{L^3}{3EI_z} + \frac{Ll^2}{GJ} \right)^{-1}. \tag{12}$$

If it is chosen as $\lambda = 0.426$ nm, for the cantilever in Figs. 7(a) and 7(b), $k_e = 94.4$ N/m. We have the critical lateral force magnitude $T_c^* = 6.4$ nN. The maximum lateral force is about 3 nN for $W = 10.0$ nN and about 10 nN for $W = 25.0$ nN (refer to Fig. 6). According to the condition in Eq. (11), stick-slip should happen in Fig. 7(b) but not in Fig. 7(a), which is consistent to our observation.

C. Methods for prevention of remarkable slow-fast tip motion

To observe the full atomic structure of the surface, the velocity of the cantilever tip should not oscillate too much during the scanning process. As pointed out earlier that this usually requires a relatively small lateral force and large lateral stiffness of cantilever. At the first thought, it seems that this can be achieved simply by applying a small normal load during measurement. However, for a typical cantilever, a small normal load means a small lateral force and therefore small cantilever flexural and twist angles (θ_y^C and θ_x^C) that may not be measured effectively due to the small signal-noise-ratio. The second thought would be to increase the lateral stiffness of the cantilever. For a rectangular cantilever, considering $G \approx E/2$ and $J \approx \frac{1}{3}bh^3$, we have

$$k_{lat} \approx \frac{Ebh}{L}\left(\frac{4L^2}{b^2} + \frac{6l^2}{h^2} \right)^{-1}, \quad k_n = \frac{Ebh^3}{4L^3}, \quad k_\theta = \frac{Ebh^3}{6Ll}, \tag{13}$$

where k_n is the vertical spring constant of the cantilever, k_θ is the twist stiffness ($\theta_x^C = k_\theta f_y$). We may increase k_{lat} by adopting the following three methods, separately or in combination: (a) increasing the cantilever width b and/or the thickness h; (b) decreasing the cantilever length L; (c) decreasing the tip length l. All of the three methods may suffer some limitations to applications. Methods (a) and (b) will increase k_n and k_θ simultaneously. Too big k_n and k_θ will lead to small θ_y^C and θ_x^C, just like the effects resulting from applying small normal load. Although method (c) has no effect on k_n, it results in an increase of k_θ. Therefore, care has to be taken to choose the cantilever geometry, tip length, and applied load so that the remarkable unsmooth tip motion does not occur and at the same time, the signal-noise ratio is big enough.

With the same normal load as that in Fig. 7(b), Fig. 7(c) shows the results with a smaller tip length $l = 2.5$ μm. As expected, the slow-fast tip motion in Fig. 7(c) becomes less remarkable than that in Fig. 7(b) and the full hexagonal lattice structure is shown in topographic map even the normal load is the same as that in Fig. 7(b). With a tip length of 2.5 μm, $k_e = 194.1$ N/m and the critical lateral force magnitude $T_c^* = 13.2$ nN. According to Eq. (11), the stick-slip motion should not occur. Actually, this was exactly what Binning *et al.*[1] did in their experiment where the full atomic structure was obtained successfully. In their experiment, a cantilever without tip was used. During measurement, the cantilever corner touched the sample surface for imaging. In the other experiment by Marti *et al.*[2] in which the full hexagonal structure of graphite surface was observed, a totally different detecting-sensing design was employed. The lateral stiffness of the wires they used is about 8×10^4 N/m, which is much stiffer than the commercially-available cantilevers whose lateral stiffness is typically 10–500 N/m.

The difficulty encountered by experimentalists in imaging the full hexagonal structure of graphite using FFM may be understood from another point of view. In FFM, topographic and friction maps are obtained simultaneously. The average lateral force in FFM measurement is defined as

$$\bar{F} = \frac{1}{t_0}\int_0^{t_0} f_y(t)dt, \tag{14}$$

where t_0 is the time that cantilever tip takes to scan over the periodic lattice structure of the surface. According to Sasaki *et al.*,[8] the appearance of a nonzero $\bar{F}$ represents the transition of the conservative lateral force to the nonconservative frictional force and indicates the occurrence of stick-slip. This means that in any FFM measurement with a nonzero $\bar{F}$, stick-slip seems to always occur. Therefore, nonzero $\bar{F}$ and topographic maps close to reality may not be obtained at the same time.

D. Image patterns due to different scan directions

In Fig. 7(d), the results are for the normal load $W=25$ nN, tip length $l=12.5$ μm, and $\alpha=30°$. Compared with Fig. 7(b), we can see the effects of scan direction on topographic and lateral force maps. Different pattern of tip paths are also shown. The differences of Figs. 7(b) and 7(d) can be explained by the different distributions of atom locations. As shown in Fig. 9, the peaks of topography for $\alpha=0°$ appear at the place where the tip is scanned between the two closely-place atoms. When $\alpha=30°$, two different areas can be distinguished. In area *A*, there is no carbon atom in the way of the scanned tip, resulting in a stripelike dark area. Area *B* is the narrow stripe where the atoms are located. Due to the unsmooth motion of the tip, the topography in this area is "averaged" and thus a stripelike bright area is shown.

Figure 7(e) shows the results for the normal load $W=25$ nN, tip length $l=12.5$ μm, and $\alpha=10°$. The stripelike topographic map is very similar to some scanning tunneling microscopy (STM) images on graphite[20] and the AFM image on boron nitride.[3] Compared with Figs. 7(b) (trigonal topography) and 7(d) (stripelike topography), Fig. 7(e) can be viewed as something between them. The scan directions of $\alpha=0°$ and 30° are two extreme cases regarding the atom location distribution. Any scan direction in the range of (0°, 30°) and (30°, 60°) should result in lateral force and topography images that are something between the results for $\alpha=0°$ and 30°. The closer α is to 0° or 60°, the more the images are similar to those in Fig. 7(b). While α is close to 30°, the resulting images should look more like those shown in Fig. 7(d).

In our simulations, surface is assumed to be rigid and atomic relaxation is not considered. As pointed out by Sasaki *et al.*,[8] atomic relaxation makes the cantilever effectively stiffer and the simulated FFM images for a cantilever without considering atomic relaxation are similar to those for a softer cantilever with the relaxation taken into account. Incorporating realistic interaction models with atomic relaxation into our model would be an important aspect of our future work.

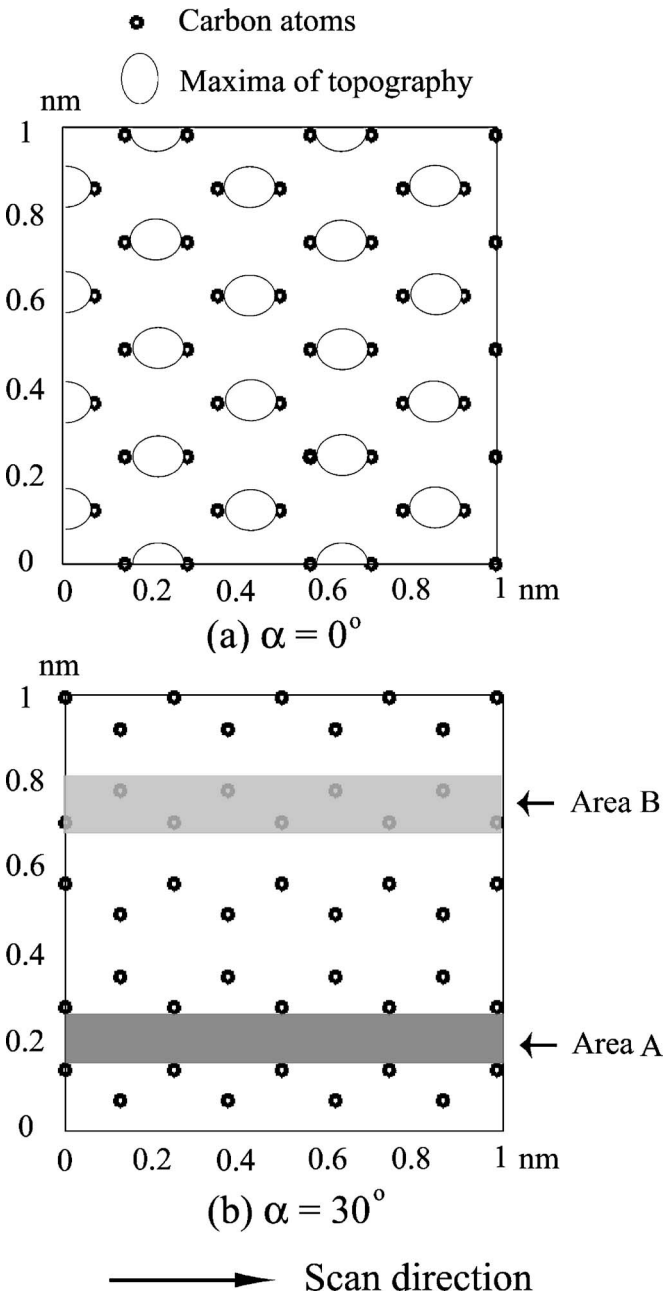

FIG. 9. (a) The relative positions of the carbon atoms in graphite surface and the maxima of topography in Fig. 7(b), when $\alpha=0°$. (b) When $\alpha=30°$, two different areas can be distinguished. In are *A*, there is no carbon atom in the way of the scanned tip. Area *B* is the narrow stripe consisting of the carbon atoms.

VI. CONCLUSION

In this paper we use a 3D FE model to simulate the atomic-scale topographic and friction force profiling process in FFM. The cantilever dynamics in operating conditions of FFM and its effects on the measured topographic and lateral force maps are investigated with different combinations of cantilever geometry, applied normal load, and scan direction.

We identify that the topographic and lateral force maps obtained in FFM experiments as the combined results of the real spatial distributions of 3D tip-sample interaction forces

and cantilever dynamics. Cantilever dynamics cannot be ignored in interpretation of FFM (and AFM) images when remarkable slow-fast tip motion is present in experiments. The experimental-obtained hexagonal and trigonal topographic images of graphite surfaces can be achieved in simulations with different combinations of cantilever geometry, applied normal load, and scan direction relative to the lattice structure of graphite. The observation of the full atomic structure of graphite surface in topographic map may be realized if the cantilever tip moves smoothly over the sample surface with a velocity that does not oscillate too much to the extent that the remarkable slow-fast tip motion occurs. This can generally be satisfied by carefully adjusting the cantilever geometry and tip length and using a relatively low applied load to ensure a relatively large cantilever lateral stiffness, a relatively small lateral force, and a reasonable signal-noise ratio. If remarkable slow-fast tip motion does occur, the appearance of trigonal or stripelike topographic maps of graphite surface depends on the scan direction. In FFM, topographic and friction maps are obtained simultaneously. However, measuring them separately may give us a better chance to obtain topographic maps close to the reality since remarkable slow-fast tip motion seems to always occur along with the measurement of a nonzero average lateral force.

We note that the presented FE model fully addresses the effects of AFM cantilever dynamics on FFM topography and friction imaging. However, in this model, the elasticity of the tip and the atomic relaxation of the tip and sample, which could play a role as important as the cantilever dynamics in the FFM topographic and friction imaging, are not considered. The more sophisticated models that account for both the cantilever-tip dynamics and atomic tip-sample relaxation are desirable in the future study.

*Corresponding author. Email address: bhushan.2@osu.edu

[1] G. Binning, Ch. Gerber, E. Stoll, T. R. Albrecht, and C. F. Quate, Europhys. Lett. **3**, 1281 (1987).
[2] O. Marti, B. Drake, and P. K. Hansma, Appl. Phys. Lett. **51**, 484 (1987).
[3] T. R. Albrecht and C. F. Quate, J. Appl. Phys. **62**, 2599 (1987).
[4] J. Ruan and B. Bhushan, J. Appl. Phys. **76**, 5022 (1994).
[5] P. Batra and S. Ciraci, J. Vac. Sci. Technol. A **6**, 313 (1988).
[6] L. Xu, X. W. Yao, L. P. Zhang, M. Q. Li, and F. J. Yang, Phys. Rev. B **51**, 10013 (1995).
[7] C. M. Mate, G. M. McClelland, R. Erlandsson, and S. Chiang, Phys. Rev. Lett. **59**, 1942 (1987).
[8] N. Sasaki, K. Kobayashi, and M. Tsukada, Phys. Rev. B **54**, 2138 (1996).
[9] H. Holscher, U. D. Schwarz, and R. Wiesendanger, Surf. Sci. **375**, 395 (1997).
[10] S. Fujisawa, K. Yokoyama, Y. Sugawara, and S. Morita, Phys. Rev. B **58**, 4909 (1998).
[11] H. Hölscher, U. D. Schwarz, O. Zwörner, and R. Wiesendanger, Phys. Rev. B **57**, 2477 (1998).
[12] J. Chen, R. K. Workman, D. Sarid, and R. Höper, Nanotechnology **5**, 199 (1994).
[13] H. J. Butt and M. Jaschke, Nanotechnology **6**, 1 (1995).
[14] U. Rabe, K. Janser, and W. Arnold, Rev. Sci. Instrum. **67**, 3281 (1996).
[15] S. I. Lee, S. W. Howell, A. Raman, and R. Reifenberger, Phys. Rev. B **66**, 115409 (2002).
[16] K. Yamanaka and S. Nakano, Appl. Phys. A **66**, S313 (1998).
[17] V. Scherer, W. Arnold, and B. Bhushan, Surf. Interface Anal. **27**, 578 (1999).
[18] M. Reinstädtler, U. Rabe, A. Goldade, B. Bhushan, and W. Arnold, Tribol. Int. **38**, 533 (2005).
[19] Y. Song and B. Bhushan, J. Appl. Phys. **97**, 083533 (2005).
[20] Y. Song and B. Bhushan, Microsyst. Technol. **12**, 129 (2006).
[21] Y. Song and B. Bhushan, J. Appl. Phys. **99**, 094911 (2006).
[22] H. Hölscher, U. D. Schwarz, and R. Wiesendanger, Europhys. Lett. **36**, 16 (1996).
[23] W. L. Wang, S. J. Hu, and R. Clarke, Phys. Rev. B **68**, 245401 (2003).
[24] Y. Song and B. Bhushan, Ultramicroscopy **106**, 847 (2006).
[25] *Springer Handbook of Nanotechnology*, edited by B. Bhushan (Springer, Heidelberg, 2004).
[26] *Nanotribology and Nanomechanics: An Introduction*, edited by B. Bhushan (Springer, Heidelberg, 2005).
[27] L. Shluger, A. I. Livshits, A. S. Foster, and C. R. A. Catlow, J. Phys.: Condens. Matter **11**, R295 (1999).
[28] K. L. Johnson and J. Woodhouse, Tribol. Lett. **5**, 155 (1998).
[29] H. A. Mizes, S. I. Park, and W. A. Harrison, Phys. Rev. B **36**, 4491 (1987).
[30] A. Selloni, P. Carnevali, E. Tosatti, and C. D. Chen, Phys. Rev. B **31**, 2602 (1985).